Formulation of polymeric particles with controlled charges by alkaline tempering

Mathis Benyaya, Marie-Alexandrine Bolzinger, Yves Chevalier, Claire Bordes

Formulation of polymeric particles with controlled charges by alkaline tempering

Mathis Benyaya [*], Marie-Alexandrine Bolzinger, Yves Chevalier, Claire Bordes [*]
Université de Lyon, Université Claude Bernard Lyon 1, CNRS UMR 5007, Laboratoire d'Automatique, de Génie des Procédés et de Génie Pharmaceutique (LAGEPP), 43 Bd du 11 Novembre 1918, 69622, Villeurbanne, France

Authors and contact: Mathis Benyaya [*] mathis.benyaya@univ-lyon1.fr
Marie-Alexandrine Bolzinger marie.bolzinger@univ-lyon1.fr
Yves Chevalier yves.chevalier@univ-lyon1.fr
Claire Bordes [*] claire.bordes@univ-lyon1.fr
[*] *: corresponding authors*

Highlights

- Anionic PMMA particles were obtained using an alkaline tempering procedure
- Surface charges are due to hydrolysis and diffusion of methacrylic acid monomers
- The tempering process was needed for the methacrylic acid to diffuse to the surface
- A core-shell particle diffusion model predicted the charges appearance kinetic

Keywords: anionic PMMA, microparticles, surface charges, PMMA, diffusion

Abstract

The control of surface charge of polymeric microparticles is a major challenge because electrostatic interactions stabilize their aqueous suspensions. In this study, anionic PMMA particles were prepared with 5 wt% of methacrylic acid as a comonomer. This comonomer was expected to give a negative charge to the particles, but none was observed from zeta potential measurements. The evolution of the zeta potential in alkaline medium was investigated to better understand this observation. It was demonstrated that the acid groups were present almost only in the core of the particles and that their deprotonation was possible using an alkaline tempering. Two phenomena occurred simultaneously leading to the charge appearance at the particle surface: i) the diffusion of hydroxide ions into the particles, allowing the migration of the negative charges to the particle surface with an appearance rate per mol of particles of 2.0 10^{-3} $m^3 \cdot mol^{-1} \cdot s^{-1}$ (multiplied by the hydroxyl ion concentration), and ii) the hydrolysis of ester groups of methyl methacrylate units characterized by a pseudo first order kinetics with k = 3.0 10^{-9} $m^3 \cdot mol^{-1} \cdot s^{-1}$. By carefully choosing the parameters of the tempering process, hydrolysis is minimized and anionic particles can be prepared with stable and controlled charges coming from the anionic comonomer. Doing so, anionic PMMA-like particles exhibited a stable zeta potential of −11.5 mV.

1. Introduction

Negatively charged polymer microparticles have been widely studied in the pharmaceutical and cosmetic fields, notably as delivery systems of active molecules (1,2). The charges stabilize the particles and keep a better homogeneity by preventing their aggregation and sedimentation (3). Several synthesis strategies of charged particles may be considered.

Neutral particles are synthetized and the surface charge is added in a further step through either binding charged molecules, surface treatment or polymer coating (4,5). In both cases, it is difficult to precisely control the charge and the surface structure of the resulting polymeric particles. A more complex technic is to polymerize another polymer on the surface of the particles, but then the entire surface properties are modified (6,7). Another strategy is the preparation of particles from polyelectrolytes. They are often synthesized using an ionic initiator. During the polymerization process, the charged groups are inserted in the polymer chains and the charge density of the particles can hardly been modified. A last strategy consists in the synthesis of a ionic copolymer, combining a neutral monomer with a comonomer carrying the charge (8). Doing so, the charge of particles obtained from such copolymer can be adjusted by the quantity of comonomer added.

This last option was chosen. However, the particles freshly prepared did not exhibit any surface charge. In the literature, a general understanding of the mechanism involved in the appearance of charges is still missing. It is the aim of this study to investigate such mechanism. For this purpose, MMA-based copolymers were synthesized in order to prepare negatively charged particles. The copolymer synthetized was then derived from poly(methyl methacrylate) (PMMA), a well-known biocompatible and non-biodegradable polymer. It is largely used for prosthesis in the medical field, for dental implants or bone reconstruction (9). There are many methacrylate comonomers that copolymerize with MMA with minor composition drift. Here, we used methacrylic acid as a comonomer to synthetize an anionic “PMMA-like” copolymer. Several syntheses using the combination of these monomers are already reported in the literature (10–12). A random distribution of the anionic comonomer is generally observed along the final polymer chain (10,12–14).

In this article, PMMA and anionic PMMA (a-PMMA) were synthetized and used to prepare microparticles. Due to the similar nature of the monomers and to the limited amount of co-monomer used (5 wt%), the two types of developed polymer particles should be biocompatible and differed only in terms of their surface charge. The charges of the particles were measured after tempering in alkaline

media at different pH. The kinetics of the charges appearance at the particle surface was determined and predicted by a specific diffusion model.

2. Experimental section

2.1. Materials

Methyl methacrylate (purity ≥ 99.0%) from Sigma-Aldrich and methacrylic acid (purity ≥ 99.5%) (MAA) from Acros Organics were used as monomers to synthetize neutral or anionic PMMA. The solvents used during these syntheses were tetrahydrofuran (purity ≥ 99.0%) purchased from Sigma-Aldrich and heptane (purity ≥ 99.0%) from VWR chemicals. 2,2'-Azobis(2-methylpropionitrile) (AIBN) from Sigma-Aldrich was used as an initiator. Ethyl acetate (purity ≥ 99.5%) from Sigma was used during the formulation of the particles to dissolve the synthetized polymer. The Mowiol 4-88 polyvinyl alcohol (PVA) purchased from Sigma-Aldrich was used as the emulsifier.

2.2. Polymer synthesis

The synthesis of PMMA and anionic PMMA was done using a classical free-radical polymerization process in tetrahydrofuran (THF) solution. Only MMA was used as monomer to synthesize neutral PMMA, while anionic PMMA (a-PMMA) was obtained by copolymerization at 60 °C of MMA and MAA monomers at 95/5 weight ratio. The reaction was performed into a reflux flask system. The solvent was firstly de-oxygenated by a nitrogen flow to prevent radical scavenging by oxygen. The monomers were then added (15 g MMA for PMMA or 14.25 g of MMA and 0.75 g of MAA for a-PMMA). 0.3 g of AIBN was used as the initiator. After 5 h of reaction, the mixture was left to cool down to room temperature before the precipitation step. The solution was added dropwise into a large amount of heptane under vigorous stirring. Heptane was chosen as the precipitation solvent as it is miscible with THF while being a non-solvent for PMMA making the polymer precipitation possible (15). The suspension was filtered on sintered glass filter to recover the polymer and then rinsed with water. Then, the polymer was vacuum-dried at 105 °C for 24 h to evaporate residual solvents. The temperature was higher than the heptane and THF boiling points (respectively 96 °C and 80 °C), but lower than the degradation temperature of PMMA (about 175 °C). The polymer was regularly crushed using a mortar with a pestle during the drying period.

2.3 Polymer characterization

^{1}H NMR analyses were made to check against the chemical structure of the copolymer and ensure that no residual monomer or solvents remained. NMR spectra were recorded on a Bruker AV400 equipped with a Bruker BBFO probe working at 400 MHz at the CCRMN of Lyon 1 University. 8 scans were measured at 60 °C in DMSO to sharpen the peaks and improve the resolution.

Differential scanning calorimetry (DSC) was performed in order to determine the glass transition temperature (T_g) of the polymers. The measurements were performed using a DSC Q200 instrument (TA Instruments; New Castle, DE). Samples were put into an aluminum crucible and analyzed using a program made of two heating cycles separated by a cooling step. The second heating scan was used for the determination of T_g. The temperature ranged between 20 °C and 120 °C (or 150 °C) with a heating rate of 10 °C min^{-1}.

2.4 Particle preparation

PMMA microparticles were obtained using an emulsion-evaporation technique. The polymer was dissolved in 10 mL of ethyl acetate. 15 mL of an aqueous solution of 0.8 wt% PVA was added. The emulsion was prepared by the means of an Ultraturax rotor-stator mixer at 24 000 rpm for 5 min. The emulsion was then added to 150 mL of distilled water and left at least for 3 h under gentle stirring to

allow the extraction/evaporation of ethyl acetate. The suspension was then cleaned 7 times by using centrifugation and supernatant replacement by water each time to remove of the PVA and the possible residual organic solvents. The particles were finally re-suspended in 40 mL of water under vigorous stirring and then dispersed by ultrasounds in a cleaning bath to break possible aggregates.

2.5. Particle characterization

The particle concentration in the suspensions was determined by measuring their dry extract weight. For each suspension, measurements were performed in triplicate.

The particle size distribution was determined by small-angle light scattering using a Malvern Mastersizer 3000 (Malvern Panalytical, UK) instrument at a stirring rate of 1400 rpm in the sample reservoir.

To verify the integrity of the particles, SEM pictures were taken. A Neoscope JCM-5000 was used with a tension of 10 kV. Magnification used was between 3 000x and 10 000x.

ζ-potential is a good indicator of the surface charges of particles. It was measured using a Zetasizer NanoZS (Malvern Panalytical, UK). 10 mL of aqueous suspension containing particles at the desired concentration was prepared. HCl or NaOH solutions were used to adjust the pH. The suspension was then diluted into water to obtain a conductivity low enough (between 1 and 4 mS cm^{-1}) to ensure reliable *ζ*-potential measurements at high ionic strength.

The evolution of *ζ*-potential as a function of the pH was measured in triplicate for PMMA and a-PMMA particles. The corresponding standard deviations (n = 3) were always about 2 mV. The kinetics of charge apparitions at the particle surface were repeated for certain operating conditions. The coefficient of variation (CV) obtained for each repeated measurement was always between 8 and 20%, with an average of 12%. A CV of 12% was thus used as a reliable estimation of the experimental error for each measurement.

An Analysis of Covariance (ANCOVA) test was performed to compare the intercepts and the slopes of the linear regression models used for the fitting of the kinetics of the surface charge appearance. The within-group variance required by the ANCOVA test was estimated from the CV values. Excel ANCOVA module was used to run the tests (See Supplementary Information 4).

2.6. Theoretical background for the determination of particle surface charge from the measured ζ-potential

A direct measurement of the surface charge of particles is complicated. This is why they were determined from *ζ*-potential values that can easily be measured by an electrophoresis experiment. The *ζ*-potential is defined as the difference of potential between the slipping plane close to the surface of the particles and the neutrality point at an infinite distance from them. The slipping plane is the separation surface between the part of the liquid medium containing bound molecules (water and ions) and free species in the bulk solution. "Bound" molecules are those moving together with the particles under the electric field of the electrophoresis experiment. Thus, the value of the *ζ*-potential depends on the surface charge of the particles, their size, and the dielectric constant of the medium. Conversion of the *ζ*-potential into surface charge density requires solving the Poisson–Boltzmann equation describing the electric potential profile with respect to distance from the center of the particles immersed in an ionic solution. The exact solution is the matter of a numerical resolution. Many analytical expressions have been proposed as solutions for this equation under various levels of approximation. They allow linking the effective charge of the particle and the measured *ζ*-potential (16–20). In this study, the equation developed by Ohshima *et al.* (17) (Eq. 1) was used. It is the most precise analytical expression for nanoparticles at low ionic strength (lower than 5 mM) (18). The surface charge density σ reads:

$$\sigma = \frac{2\epsilon_0\epsilon_r\kappa k_b T}{e}\sinh\left(\frac{e\zeta}{2k_bT}\right) * \left[1 + \frac{1}{\kappa R_p}\frac{2}{\cosh^2\left(\frac{e\zeta}{4k_bT}\right)} + \frac{1}{(\kappa^2 R_p^2)}\frac{8\ln\left(\cosh\left(\frac{e\zeta}{4k_bT}\right)\right)}{\sinh^2\left(\frac{e\zeta}{2k_bT}\right)}\right]^{\frac{1}{2}} \quad \text{(Eq. 1)}$$

with ϵ_0 the permittivity of vacuum, ϵ_r the relative permittivity of the solution (water), κ the Debye-Hückel parameter, k_B the Boltzmann constant, T the absolute temperature, e the elementary charge, R_p the radius of the particles and the ζ-potential of the particles (all expressed in SI units).

The relation is valid upon the several hypotheses that follow. The electrolyte has to be a 1:1 electrolyte, the particles have to be spherical, and the ζ-potential has to be small enough (lower than 25 mV). For symmetrical electrolytes, κ is given by:

$$\kappa = \left(\frac{2\,N_a e^2 I}{\epsilon_0\epsilon_r k_b T}\right)^{\frac{1}{2}} \quad \text{(Eq. 2)}$$

where I is the ionic strength of the solution defined as $I = \frac{1}{2}\Sigma z_i^2 c_i$ with i referring to the ions present in the solution. As the only ions present were Na^+ and HO^- in equal concentration, c_i can be deduced from conductivity measurements. Indeed, the conductivity is $\eta = \sum c_i\eta_i$ with η_i the molar ionic conductivity of each ion. The average molar conductivity of Na^+ and HO^- is η_a= 125 mS L cm^{-1} mol^{-1}. Then $I = \frac{\eta}{2\,\eta_a}$.

The surface charge $z_{particle}$ of a single particle can also be deduced from (Eq. 1) as:

$$z_{particle} = 4\pi R^2\sigma \quad \text{(Eq. 3)}$$

with R being the particle radius and σ the electric charge density of the particles obtained from Eq. 1. The Smoluchowski approximation of the Henry relationship was used to calculate the ζ-potential from the measured electrophoretic mobility μ:

$$\mu = \frac{\epsilon_0\epsilon_r\zeta}{\eta} \quad \text{(Eq. 4)}$$

This approximation is only valid for large κR_p (> 100), i.e. for particles larger than 0.2 μm, and dispersed in an aqueous salt solution of concentration above 10^{-3} M, which is the present case.

3. Results and discussion

3.1. Polymer analysis

^{1}H NMR analysis confirmed that the polymerization occurred and that no residual monomer was present in the final product (PMMA or a-PMMA) (Figure S1). The disappearance of the two peaks characteristic of the vinyl function of the monomer at 5.2 and 5.7 ppm was observed, while a peak at 3.6 ppm typical of PMMA has appeared. It is worth noting that, for the a-PMMA, the hydrogens of the carboxylic acid group are not easily detectable because their content in the copolymer is low (5% MAA) and peaks of labile hydrogens are broad.

Table 1. Theoretical and experimental values of the glass transition temperature for each polymer.

	% of MMA (w/w)	**% of co-monomer (w/w)**	**T_g (°C)** *Theoretical*	**T_g (°C)** *Measured*
PMMA	100%	0%	105	99
a-PMMA	95%	5%	108	119

PMMA glass transition temperature (T_g) is very dependent on the tacticity of the polymer. The isotactic polymer has a T_g of about 43 °C, the syndiotactic one is around 123 °C, and the atactic PMMA is around 100 °C (21). There is a large variability of reported values spanning 15 °C. As example, other authors reported a T_g about 61 °C for the isotactic-polymer, 114 °C for the atactic polymer and 131 °C for the syndiotactic-polymer (22). The experimental results were compared to theoretical values

obtained by using the comonomer T_g. A maximum difference of 15 °C between predicted and experimental T_g values was acceptable to validate the nature of the synthesized polymer (Table 1). To determine the theoretical T_g of a-PMMA the Fox equation was used (23).

$$\frac{1}{T_g} = \sum\left(\frac{w_i}{T_{g_i}}\right) \quad \text{(Eq. 5)}$$

with T_g the glass transition temperature of the copolymer, w_i the mass ratio of each co-monomer in the mixing, and T_{g_i} the glass transition temperature of each pure polymer based on these monomers.

The experimental T_g values of 99 °C and 119 °C were obtained from the DSC thermograms measured for PMMA and a-PMMA polymers, respectively (Figure S2). The reference T_g values were obtained from the Polymer Handbook, i.e. 105 °C for pure PMMA and 228 °C for pure PMAA (Table 1) (24). Due to the consistency of the results, it was considered that both polymers were successfully synthetized and that the distribution of methacrylic acid groups was at random along the polymer chains.

3.2. Particles analysis

3.2.1. Particle size and concentration of the suspensions

The mass concentrations of the particles in the suspensions were 1.67 wt% (±0.07%) for PMMA and 2.38 wt% (±0.09%) for a-PMMA. The obtained particles exhibited similar size distribution with a median diameter D(50) of 0.67 µm for PMMA particles (Span of 1.36) and 0.75 µm for a-PMMA (Span of 1.12).

3.2.2. Contamination by PVA

The particle preparation process required PVA as stabilizer. To avoid any influence of this surfactant during the rest of the study, a particle washing protocol was developed based on several successive rinsing steps. At each step, the surface tension of the washing water was measured in order to determine the amount of residual PVA. A calibration with aqueous solutions containing different concentrations of PVA ranging from $5\ 10^{-2}$ to $5\ 10^{-5}$ % w/w (Figure 1) allowed the estimation of the concentration of residual PVA. Below $5\ 10^{-5}$ %w/w PVA, no significant difference was observed between the surface tensions of the PVA solution and pure water. The presence of particles in suspension did not interfere with the measurements. Indeed, solid particles are generally considered to have no influence on water surface tension (25). To check against this, the surface tension of the washing waters were measured before and after centrifugation at 10 000 rpm that caused sedimentation of any residual PMMA particles. No difference was observed (results not shown). The residual PVA was undetectable after 6 washing steps (Figure 1).

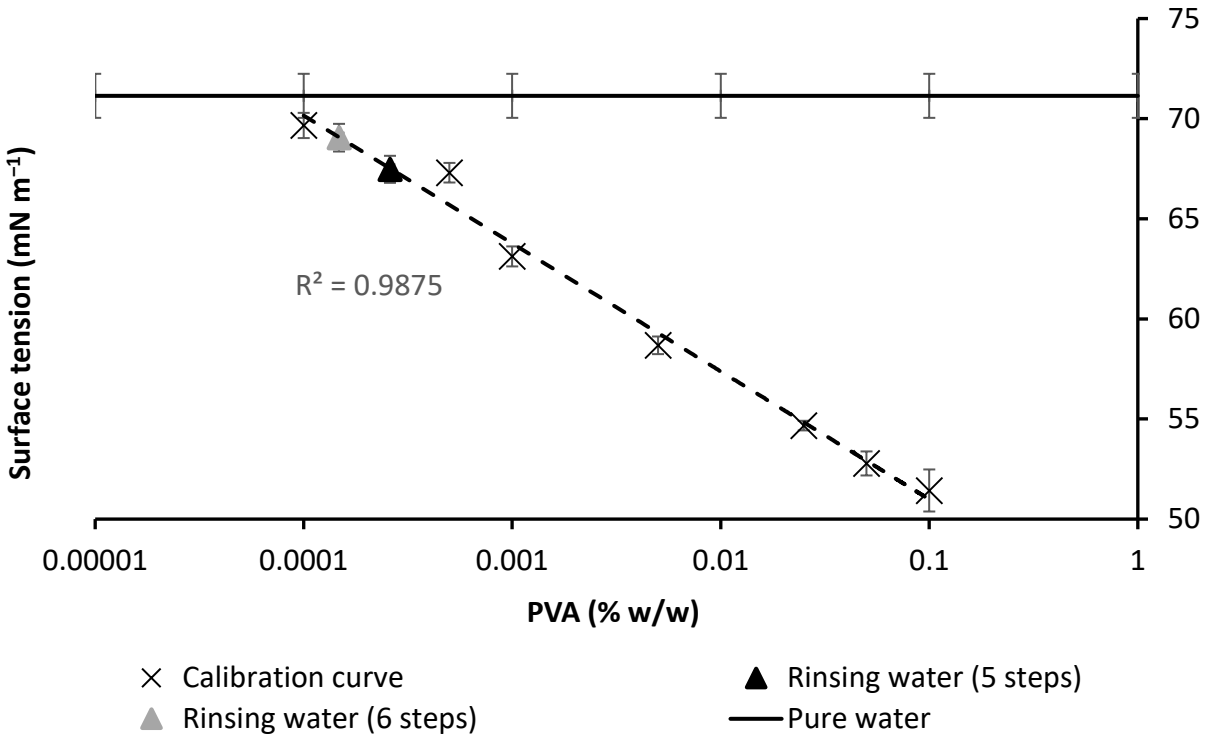

Figure 1. Surface tension of the washing waters after the rinsing of the particles. Aqueous solutions of PVA were used to obtain the calibration curve (dashed). Each measurement was done in triplicate and results are presented as means ± SD.

3.2.3. ζ-potential of the neutral PMMA particles

The *ζ*-potential increases (in absolute value) with respect to the particle charge, but the relationship between them is far from being linear. The measured *ζ*-potential is independent from the particle concentration in the sample. In these experiments, the surface charges were presumed essentially due to the deprotonated acid groups of the MAA comonomer located at the surface of the particles. The potential should be null for PMMA that does not contain such acid groups. For a-PMMA, as the p*K*a of poly(methacrylic acid) is 4.8, the maximum charge of the particle was expected to be reached above pH 6. On the other hand, a null potential should be observed at pH lower than 3. A negative and pH-dependent ζ-potential was therefore expected.

Figure 2 represents the *ζ*-potential of PMMA particles at different pH. The ζ-potential was close to zero for pH ranging from 2 to 11 (slightly negative around −0.9 mV in acidic medium and around −1.5 mV in basic medium). An almost null ζ-potential suggested the absence of surface charge, even at approaching the basic pH 11. These results are in good agreement with the literature even though the comparison remains difficult due to the dependence of the ζ-potential on the ionic strength (26). At pH above 11.5, the *ζ*-potential sharply decreased by increasing the pH. During the experiment, the particle *ζ*-potential was measured 1 h, 24 h and 48 h after the preparation of the suspension. For pH greater than 10.5, the *ζ*-potential was time-dependent (Figure 2). Moreover, the longer the particles stayed in alkaline medium, the higher the potential was in absolute value. The higher the pH, the larger the *ζ*-potential and the time-drift of the *ζ*-potential were. This phenomenon was interpreted as coming from the hydrolysis of the ester functions occurring at high concentrations of hydroxyl ions at the surface of the particles.

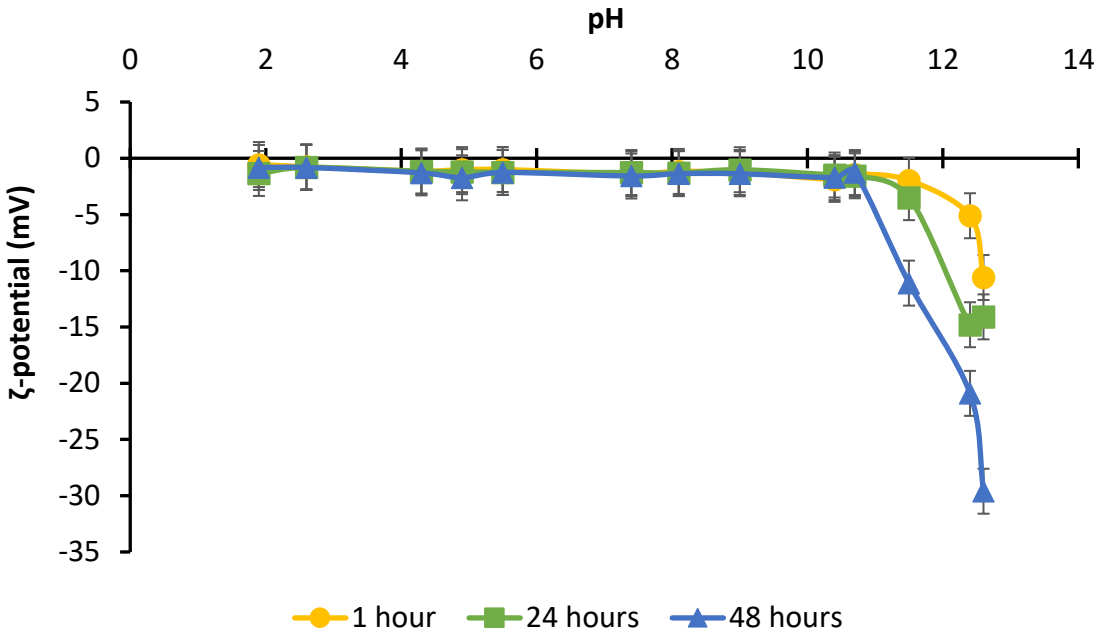

Figure 2. ζ-potential of PMMA particles as a function of the pH. The measurements were performed immediately after preparation and after 1 day and 2 days left at the chosen pH. Each measurement was done in triplicate and results are presented as means ± SD.

To further investigate this hydrolysis phenomenon, the time evolution of ζ-potential was followed for PMMA particles in aqueous solutions at different pH and for two different particle concentrations. The quantity of hydrolyzed functions was calculated from the charge generated by the hydrolysis reaction; the latter being determined using ζ-potential measurements and Eq. 3.

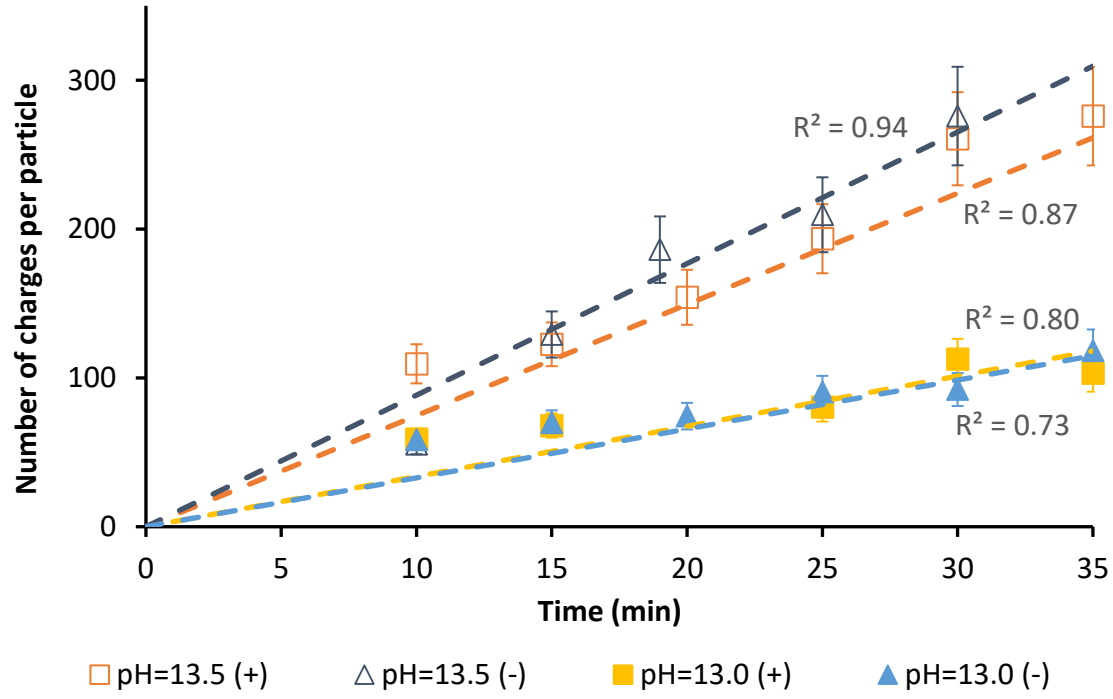

Figure 3. Time evolution of the ester function hydrolysis in PMMA particles. The number of charges that appeared at the particle surface corresponds to the number of hydrolyzed functions. (-) refers to a particle concentration of 0.02 g L^{-1} and (+) to a concentration of 0.04 g L^{-1}. Results are presented as means ± (mean*CV).

3.2.4 Hydrolysis mechanism

Prior to the use of Eq.3 for the determination of z_{eff}, ζ-potential values were corrected by subtracting the ζ-potential of PMMA particles in alkaline solution, i.e. −1.5 mV. Finally, the time evolution of the effective charge of PMMA particles allowed determining the kinetics of the ester function hydrolysis (Figure 3). As shown in Figure 3, the charge evolved linearly with respect to time, indicating a constant rate of hydrolysis over the first 45 min. The higher the pH and the particle concentration, the faster the hydrolysis rate. The mechanism of the hydrolysis reaction was analyzed more precisely. The reaction of hydrolysis of ester groups in basic medium can be written as:

$$\mathrm{RCOOCH_3} + \mathrm{HO^-} \rightarrow \mathrm{RCOO^-} + \mathrm{CH_3OH}$$

The reaction was irreversible (27) because the very few released methanol cannot cause the reverse reaction in aqueous medium. In this study, the advancement of the reaction was always below 1% of the initial ester concentration. As the volume was constant, the kinetics of the hydrolysis reaction can be written as being first order with respect to each reagent:

$$v = \frac{-\mathrm{d[RCOOCH_3]}}{\mathrm{d}t} = \frac{\mathrm{d[RCOO^-]}}{\mathrm{d}t} = k[\mathrm{RCOOCH_3}][\mathrm{HO^-}] \quad \text{(Eq. 6)}$$

with v the reaction rate in mol L^{-1} min^{-1}, k the kinetic constant expressed in L mol^{-1} min^{-1}.

As the pH ranged from 12 to 14, $[\mathrm{HO^-}]$ was between 0.01 and 1 mol L^{-1}. From the advancement lower than 1% and the initial concentration of the polymer smaller than 10 g L^{-1} (= 0.1 mol L^{-1}), the maximum $\mathrm{HO^-}$ concentration variation was around 0.001 mol L^{-1}, so that $[\mathrm{HO^-}]$ could be considered as constant during the hydrolysis reaction of these experiments. For such low reaction advancement, the structure of the particles was expected to be preserved and k is a constant. In these conditions, the Eq. 6 can be solved as:

$$[\mathrm{RCOOCH_3}](t) = [\mathrm{RCOOCH_3}](0)\ \mathrm{e}^{-k[\mathrm{HO^-}]\,t}$$

As $[\mathrm{RCOO^-}](t) = [\mathrm{RCOOCH_3}](0) - [\mathrm{RCOOCH_3}](t)$, it can be deduced:

$$[\mathrm{RCOO^-}](t) = [\mathrm{RCOO^-}](0)\left(1 - \mathrm{e}^{-k[\mathrm{HO^-}]\,t}\right)$$

The exponential term being much smaller than 1, a series development limited to first order gives:

$$[\mathrm{RCOO^-}](t) = [\mathrm{RCOOCH_3}](0)\ k[\mathrm{HO^-}]\ t \quad \text{(Eq. 7)}$$

According to the assumptions above, the pseudo-first order reaction model predicts the observed linear variation of the concentration of charged groups with respect to time. This hydrolysis model was already used by many authors in cases of different polymers: polyacrylamide at high pH (28), poly(D,L-lactide) at pH 11.4 (29) or PLGA for drug delivery systems (30,31). These authors also observed a pseudo-first order reaction at low advancement which is in good agreement with the results obtained here for PMMA particles. The values calculated for the rate constant k and the corresponding determination coefficients are reported in Table 3.

Table 3. Reaction rate constant of the ester hydrolysis at the surface of the PMMA particles.

Particle concentration (mol m^{-3})		**pH / $[\mathrm{HO^-}]$ (mol m^{-3})**	**k (m^3 mol^{-1} s^{-1}) (x10^{-9})**	**R^2**
Theoretical value: 20	19.23	13.5 / 315	2.9	0.87
	20.19	13.0 /99	3.3	0.73
Theoretical value: 40	39.18	13.5 / 316	2.5	0.94
	39.81	13.0 / 101	3.5	0.80

The average rate constant is k = 3.0 10^{-9} m^3 mol^{-1} s^{-1} (Figure S3). It is worth noticing that the value of R^2 for the hydrolyzed particles was lower at the lower pH (13). At pH 13, the limited hydrolysis phenomenon was characterized by low ζ-potential values (in absolute value) that are associated with the more important measurement error.

3.2.5. ζ-potential of the a-PMMA particles

The ζ-potential measurements of the a-PMMA particles gave unexpected results. As mentioned before, the ζ-potential was expected to be negative due to the deprotonated acid groups at the surface of the particles. Considering spherical particles and a random distribution of the acid monomers inside particles, the number of monomers present at the surface can be estimated. A spherical particle contained $n_{tot} = \frac{m_{particle}}{m_{monomer}} = \frac{\rho\, V_{particle}}{m_{monomer}}$ with ρ the density of PMMA i.e. 1.18 g cm^{-3}. The volume of a monomer is then equal to $V_{monomer} = \frac{V_{particle}}{n_{tot}}$. Finally, the number of monomers at the surface of the particle is equal to the surface of a particle divided by the cross-section area of a monomer, which is equal to its volume multiplied by 2/3.

$$n_{surface} = \frac{4\pi R_p^2}{\left(\frac{V_{particle}}{n_{tot}}\right)^{\frac{2}{3}}} = \frac{4\pi R_p^2}{\left(\frac{m_{monomer}}{\rho}\right)^{\frac{2}{3}}} \qquad \text{(Eq. 8)}$$

with R_p the particles radius.

The molar ratio between MAA and MMA being 5.8, Eq. 8 gives the number of acid functions present at the surface of one particle: $n_{acid\ at\ the\ surface} = 5.8\% \times n_{surface} \approx 50\,000$. Being at the particle surface, these carboxylic groups should be quickly deprotonated in alkaline medium, yielding a large surface charge. But the ζ-potential of a-PMMA particles was very low over a wide pH range (from 4 to 10), identical to that measured for PMMA particles. The very low ζ-potential absolute value indicated that there was almost no charged groups at the surface of the particles. Therefore, the methacrylic acid units were buried inside the particle core. At pH about 11.5, a low ζ-potential was measured immediately after the particle preparation (about −5 mV). After 6 days, its absolute value increased and reached −32 mV, against −12 mV for the PMMA particles (Figure 4). Such a behavior confirmed that the negative charged particles could only be obtained at pH higher than 11, and after a long time of incubation in an alkaline medium.

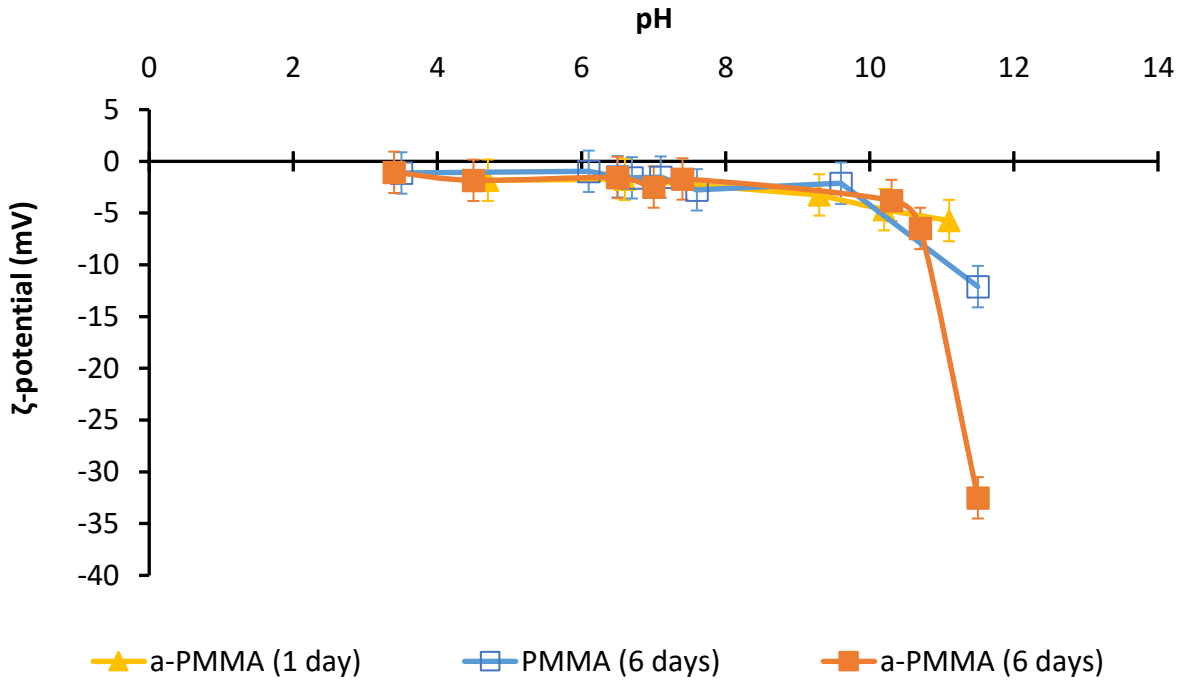

Figure 4. ζ-potential measured after 6 days storage of a-PMMA and PMMA particles as a function of pH. The ionic strength of the suspensions used for the measurements are the same. Each measurement was done in triplicate and results are presented as means ± SD.

The PMMA hydrolysis reaction being the same for PMMA and a-PMMA particles, the larger ζ-potential reached for a-PMMA particles at high pH and long incubation time came from the neutralization of the carboxylic acids of the MAA comonomer. Thus, two mechanisms simultaneously occurred during the alkaline treatment. The first one was the same ester hydrolysis as for PMMA. The second one was related to the appearance of charges of the sodium carboxylate groups of the MAA comonomers due to the deprotonation of their acid groups. The mechanism of neutralization of the carboxylic acids that caused the appearance of charged groups at the surface of particles looks tricky. Indeed, it should include several steps of diffusion of Na^+ and HO^- ions into the polymer particles for the neutralization reaction generates the sodium carboxylate groups, followed by their migration to the particle surface and finally dissociation of the ion pairs in the contact of water.

In order to address this mechanism, measurements of ζ-potential versus time at different pH and particle concentrations of a-PMMA were performed. The Ohshima's formula (Eq. 3) was once again used to calculate the charges of the particles from their ζ-potential (Figure 5). Considering that hydrolysis appeared in a similar manner for PMMA and a-PMMA particles, charges due to hydrolysis (measured with PMMA) were subtracted from those measured with a-PMMA, so as to de-correlate both phenomena.

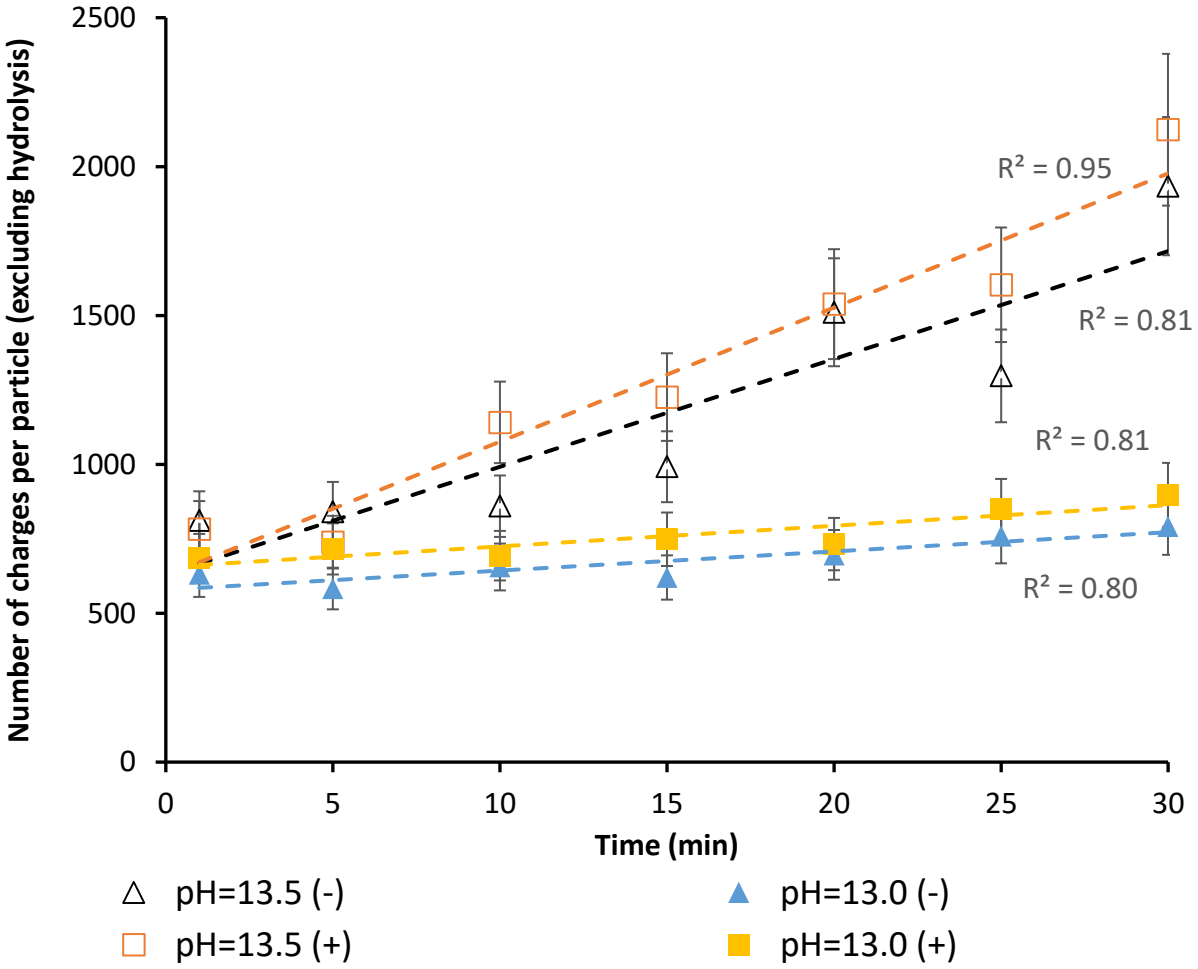

Figure 5. Kinetics of charges appearance at different pH and particle concentrations for a-PMMA. (-) refers to a particle concentration of 0.02 g L^{-1} and (+) of 0.04 g L^{-1}. Charges appearance has been determined after subtraction of charges coming from hydrolysis. The dotted line corresponds to a simple linear regression model. The results for pH of 13.2 and 12.5 were similar and were not represented on the graphic for better readability. Results are presented as means ± (mean*CV).

Figure 5 presents the time evolution of the number of charges per particle that appeared at the particle surface at pH 13, 13.2 and 13.5 for 2 different particle concentrations. Once again, the appearance of charges increased linearly with time over the first 30 min. This effect increased with the pH and the same correlation with the concentration of particles can be seen.

Table 4. *y*-intercept and slope of the linear regression models used to predict the charges appearance at different pH for a-PMMA (after subtraction of the hydrolysis phenomenon).

Particles concentration (mol m^{-3})	pH	HO^- concentration (mol m^{-3})	Slope (mol s^{-1} per particle) ($x10^{-25}$)	*y*-intercept (mol per particle) ($x10^{-22}$)	R^2
Theoretical value: 20	13.5	315.8	10.0	10.5	0.81
	13.2	158.9	4.16	8.12	0.93
	13.0	100.9	1.78	9.60	0.80
	12.5	33.2	0.70	6.06	0.56
Theoretical value: 40	13.5	318.8	12.5	10.4	0.95
	13.2	160.6	3.88	7.74	0.82
	13.0	101.1	1.91	9.22	0.81
	12.5	33.1	2.86	12.9	0.57

The slope and *y*-intercept (normalized per particle) of the linear regression models determined for the different operating conditions are given in Table 4. As observed previously, the determination coefficient decreased when the pH is too low because the corresponding ζ-potential values became comparable to the precision of the measurements. As a result, for pH of 12.5, the slope was not significantly different from 0 (*p*-value > 0.05 for the analysis of covariance by an ANCOVA test).

From a statistical point of view, the y-intercept values were considered as constant. Conversely, the slopes were significantly different as determined with the ANCOVA test using a 95% confidence interval. As said before, the charges appearance was slower by diminishing the pH value. Figure 6 represents the slopes as a function of the hydroxyl ion concentration. It indicates a linear positive relationship between the slopes and the $[HO^-]$ concentration in the bulk with a determination coefficient R^2 = 0.88.

To be able to obtain charged particles with a minimal hydrolysis phenomenon, about 20 mL of the suspension were kept at pH 13.5 for approximately 10 min. Then 200 mL of distilled water were added to quickly lower the pH. The suspension was centrifuged and the alkaline water was replaced by pure water. The process was repeated four times so as to obtain a suspension at a neutral pH. Doing so, the number of charges created by hydrolysis was reduced to a negligible extent in comparison to those coming from the deprotonation of acid groups. ζ-potential measurements were then performed for pH ranging from 4 to 12. The measurements were made immediately after the final pH adjustment down to neutral, and then after 2 and 7 days. The ζ-potential obtained was around −12 mV at neutral pH proving that the particles were effectively charged. No difference was observed after one-week storage (Figure 7). Then, the tempering in an alkaline medium seems to be a good way to make charges definitively appear.

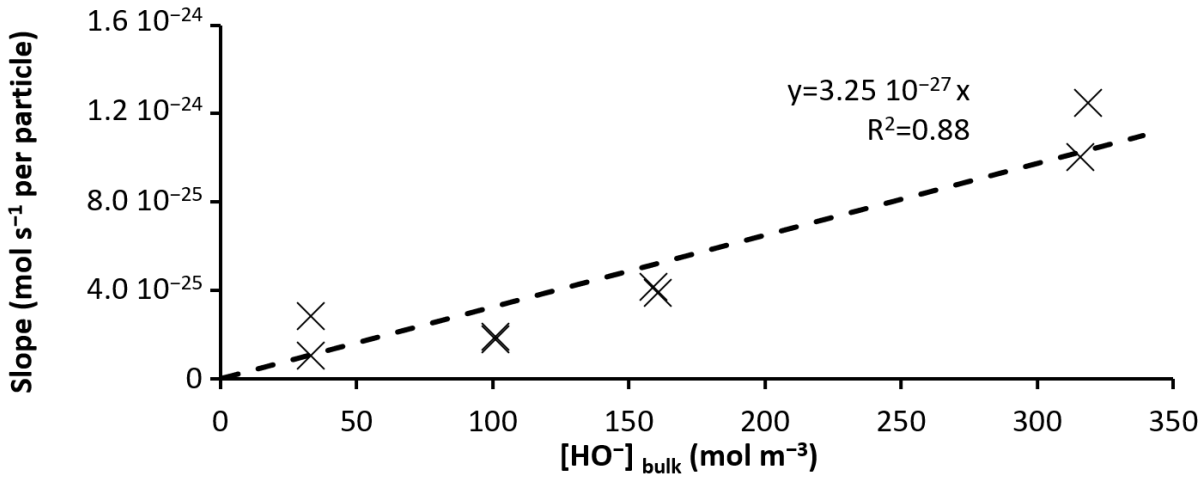

Figure 6. Slopes of the charges appearance (determined from Figure 5) as a function of the concentration of HO^- in the aqueous phase.

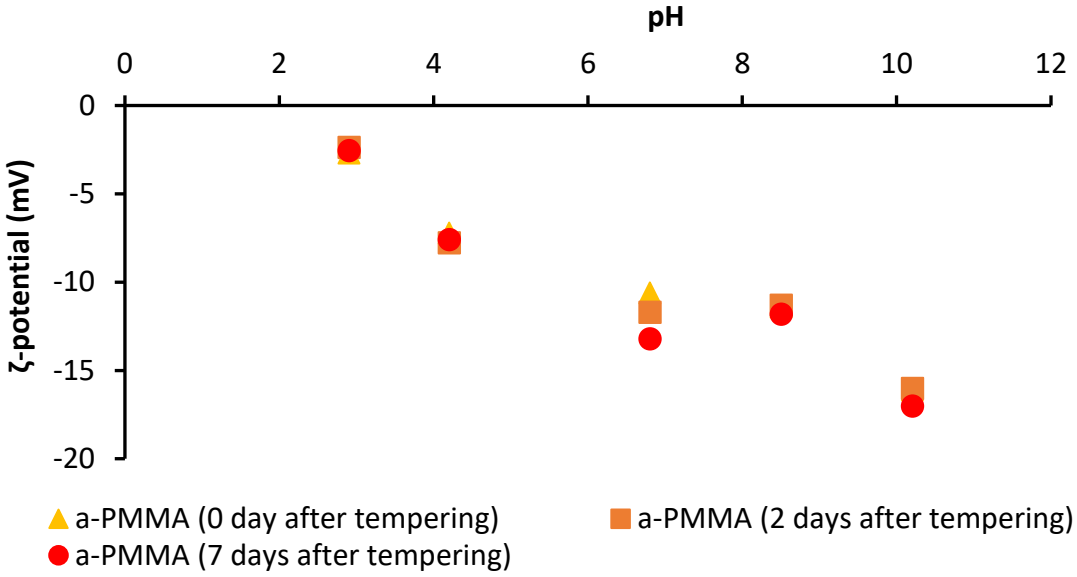

Figure 7. ζ-potential after the tempering of the particles.

3.2.6. Integrity of the particles

MEB pictures of a-pmma before and after an alkaline treatment were performed. No difference was seen between them. The particles are spherical, and no surface degradation was noted. Then, the alkaline treatment doesn't seem to degrade the particles (Figure 8).

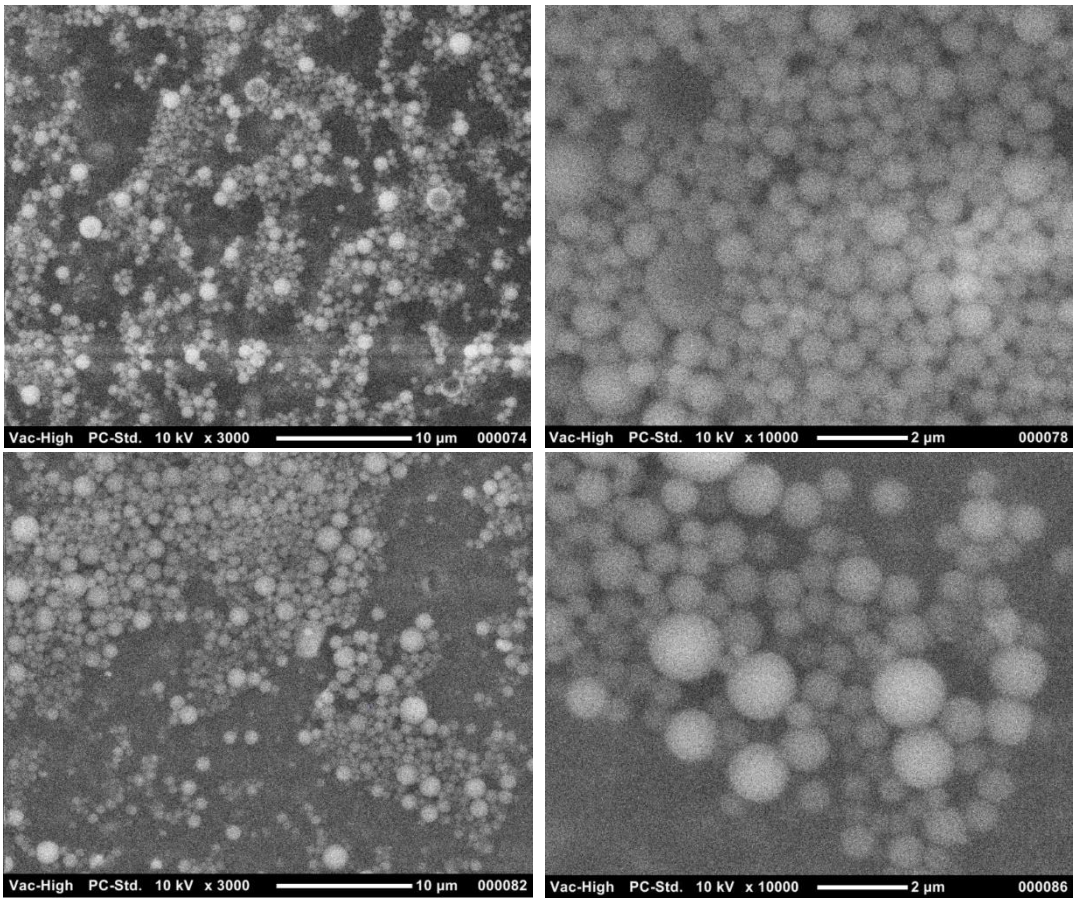

Figure 8. SEM pictures of a-pmma before (top) and after (bottom) alkaline treatment. Pictures were taken at a magnification of 3 000x (left) and 10 000x (right).

3.2.7. Mechanism of the charge appearance

The previous section disclosed that charges appeared at the polymer particle surface according to two distinct phenomena: ester function hydrolysis and MAA charge appearance. To explain this latter phenomenon, a diffusion model was proposed.

The experiments showed the charge of the particles was about 100–1000, which was quite far from the one expected (≈ 50 000). This indicates that very few acid groups were actually present at the particle surface even after the alkaline treatment. The great majority of the carboxylic acid groups of the MAA comonomer were then buried inside the particles. The particle surface was depleted of the MAA, resulting in a core-shell internal structure of the particles. Emulsion-evaporation technics were already used to create core-shell polymer particles (32). Therefore, a two-layers core-shell model of a-PMMA particles with a core containing nearly all the MAA comonomer units and a shell made of almost pure PMMA devoid of MAA was used to represent the particles (Figure 9). Such an internal structure of the microparticles may look surprising owing the emulsion-solvent evaporation process used for the preparation of the particles. Indeed, the most polar MAA units should have been located at the surface of the oil droplets of the o/w emulsion. The present experimental results showing the nearly zero ζ-potential at basic pH definitely demonstrated that the particle surface did not contain significant amounts of carboxylic acid. As experimentally observed, the shell contained very few acid monomers; their concentration is denoted c_L (for c_{Low}). The core of radius r_c contains the rest of the MAA comonomers, the acid concentration in the core is denoted c_H (for c_{High}). The particle core contains MAA under its acidic form because there were no basic compounds added for the preparation of the microparticles.

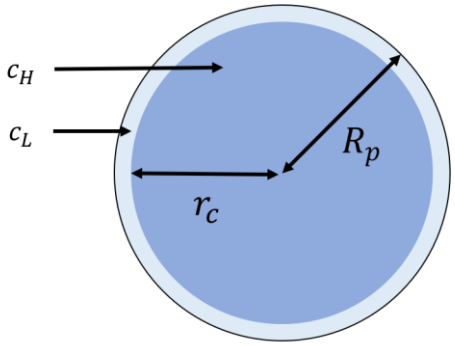

Figure 9. Schematic representation of a-PMMA particles. The acid monomers are mostly contained in the particle core.

This core-shell representation was then used to predict the charges appearance at the particle surface. The few acid functions contained into the particle shell were assumed to be immediately deprotonated. At the opposite, the appearance of the charges due to the MAA present in the core were supposed to be due to two diffusion mechanisms.

Firstly, the HO^- ions diffused from the surface to the core through the polymer matrix. As HO^- ions reached the core, they were consumed by their reaction with carboxylic acid groups and were converted into carboxylate charged groups. Secondly, the carboxylate groups linked with a Na^+ anion as ion pairs migrated from the core to the surface. Such process may be very slow because the room temperature is far below the T_g of the polymer. It was presumed that the water present in the particles acted as a plasticizer.

These two diffusion phenomena were compared with the help of the diffusion coefficients of the diffusing species. The diffusion coefficient of another salt, NaCl, was already measured in different polymeric membranes made of PMMA copolymers similar to a-PMMA (33). In particular, the diffusion coefficient of NaCl in a 85/15 copolymer of MMA and glycidyl methacrylate (GMA) was the closest to the present case. The diffusion coefficient was *D*[P(MMA/GMA) (85/15)] = 2 10^{-13} m^2 s^{-1}. The diffusion coefficient of pure water in pure PMMA determined by Unemori gave similar values about 10^{-12} m^2 s^{-1} (34). As both NaOH and NaCl are similar ion pairs, it was assumed that $D_{NaOH\ in\ PMMA} \approx 10^{-13}$ m^2 s^{-1}.

$D_{RCOONa\ in\ PMMA}$ depends on the self-diffusion of polymeric chains in the particles. Zhang *et al.* have studied the diffusion of two PMMA at a polymer/polymer interface. The diffusion has been measured at temperatures between 180 °C and 240 °C at which the polymer is in viscous state (35). The values are in between 10^{-18} and 10^{-16} m^2 s^{-1}. Below the glass transition temperature, the diffusion coefficients were even smaller, being measured around 10^{-20} to 10^{-24} m^2 s^{-1} (36,37). Thus, it can be considered that the diffusion of HO^- through the particle is instantaneous compared to the diffusion of the deprotonated group from the core to the surface. Thus, only the second diffusion mechanism was considered in the model of charge appearance.

First, the appearance of the charges due to the acid groups contained in the shell was calculated. It was considered that the such acid groups almost instantaneously reached the surface. Indeed, they are the first functions to be deprotonated and the movements of the polymer chains are easier close to the surface. Then, during an alkaline treatment, for a single particle, there is an instantaneous appearance of a number of charges n_{shell} equal to:

$$n_{shell} = \int_{r_c}^{R_p} c_L dV = \frac{4}{3}\pi\left(R_p^3 - r_c^3\right)c_L = \frac{4}{3}\pi R_p^3\left(1 - \left(\frac{r_c}{R_p}\right)^3\right)c_L \quad \text{(Eq. 9)}$$

Then the appearance of the charges due to the few acid groups contained in the core was calculated. When the deprotonated acid functions are buried into the particles, they are linked to Na^+ counter-ions as neutral ion pairs in the polymer matrix. The concentration $[RCOO^-]$ in the particle is noted c_a. To evaluate it, the diffusion of Na^+ ion was considered. As diffusion of NaOH is instantaneous,

it can be considered that $[\mathrm{Na^+}]_{in\ the\ particles} = [\mathrm{Na^+}]_{in\ the\ bulk} = c_0$ at any time. But into the particles, part of these ions is linked to acid groups and part to hydroxyl ions. Then in the particle $[\mathrm{Na^+}] = c_0 = c_a + [\mathrm{HO^-}]$. The ratio $\frac{c_a}{c_0} < 1$ is noted *K* and then: $c_a = Kc_0$.

This diffusion phenomenon has been put in formal form using Fick's law for diffusion. Diffusion through the membrane of a hollow sphere is analogous to the diffusion through a flat sheet. As almost very few acid groups are present at the surface at any time [RCOONa](*R*) = 0. [RCOONa](r_c) was considered as constant and equal to c_a as a very few functions are diffusing as far as the surface. When a stationary diffusion regime is reached, it can be written:

$$\frac{\mathrm{d}}{\mathrm{d}r}\left(r^2 \frac{\mathrm{d}c_{\mathrm{RCOONa}}}{\mathrm{d}r}\right) = 0$$

$$c_{RCOONa}(r) = c(r) = c_a \frac{r_c}{r} \frac{r-R_p}{r_c-R_p} = Kc_0 \frac{r_c}{r} \frac{r-R_p}{r_c-R_p} \qquad \text{(Eq. 10)}$$

with c_0 the concentration of $[\mathrm{HO^-}]$ in the bulk aqueous phase, and r = 0 being the centre of the particle. This is represented in Figure 10.

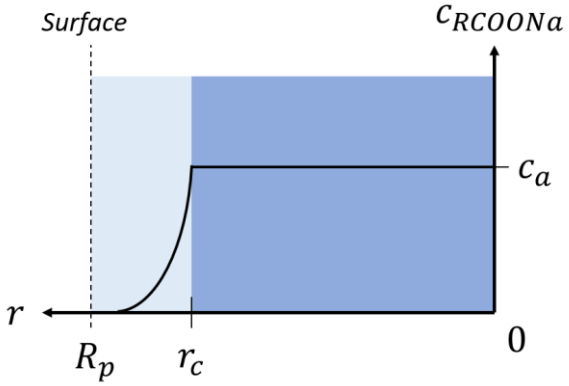

Figure 10. Representation of the concentration of RCOONa in a particle described by a core-shell system during the diffusion. The dark blue core is located at the right side along the *x*-axis from $r = 0$ to $r = r_c$, the light blue for r between r_c and R_p represents the shell, and the extreme left is the aqueous medium.

A flux of deprotonated acid groups is created from the core through the shell to the surface. This creates a time dependent effective charges for the particles. The number of charges which appeared for a single particle is:

$$n(t) = n_{core}(t) + n_{shell}(\emptyset)$$

with $n_{core}(t)$ the diffusing acid functions through the shell. The application of the Fick's law gives:

$$n_{core}(t) = \oint \int_0^t J(r) dA\, d\tau = 4\pi R_p^2 J(R_p) t$$

and with:

$$J(r) = -D_{RCOONa} \frac{dc}{dr} = \frac{D_{RCOONa}\, R_p\, r_c\, K\, c_0}{(R_p - r_c)\, r^2}$$

The appearance of charges for a single particle can be noted:

$$n_{core}(t) = 4\pi R_p \frac{r_c}{R_p} \frac{D_{RCOONa}\, K}{(1 - \frac{r_c}{R_p})}\, c_0 t$$

Finally, the total number of charges predicted for a single core-shell particle, is:

$$n(t) = 4\pi R_p \frac{r_c}{R_p} \frac{D_{RCOONa}}{(1 - \frac{r_c}{R_p})}\, K\, c_0 t + \frac{4}{3}\pi R_p^3 \left(1 - (\frac{r_c}{R_p})^3\right) c_L$$

$$= \mathrm{A}\, c_0\, t + \mathrm{B} \qquad \text{(Eq. 11)}$$

with $c_0 = c_{HO^-}$ in the bulk aqueous medium, and A and B being constants independent of time, particles concentration and c_0.

This model was used to predict the time evolution of the surface charges for a-PMMA particles and its predictions were compared to the experimental results. According to Figure 5 and Table 4, the number of charges created was proportional to the particle concentration and the charge linearly varied with time. As the *y*-intercepts of the curves divided by the number of particles were constant, the charges appearance for a single particle can be written:

$n_{particle}(t) = \alpha t + \beta$

Moreover, according to Figure 6, α is proportional to the concentration of HO^- in the bulk. So, the experimental data can be written:

$n_{particle}(t) = \alpha' c_0\, t + \beta$ (Eq. 12)

The forms Eq. 11 and 12 are identical, so that the model agrees with experiments, and $\alpha' = A$ and $\beta = B$. Numerical values were calculated for checking against the validity of the model and getting more insight into the mechanisms.

Numerical applications

Using the slope from Figure 6 and the *y*-intercepts from Figure 5, it can be deduced that:

$4\pi R_p \frac{r_c}{R_p} \frac{D_{RCOONa}\, K}{(1-\frac{r_c}{R_p})} = \alpha = 3.25\ 10^{-27}\ \frac{m^3}{s}$ (Eq. 13)

$\frac{4}{3}\pi R_p^3 \left(1 - (\frac{r_c}{R_p})^3\right) c_L = 9\ 10^{-22}$ mol (Eq. 14)

As there is no information available about the precise value of D_{RCOONa} and r_c, they were estimated and discussed to assess the reliability of the developed model.

Estimation of r_c

The size of the particle core has geometrical limitations. In one most extreme case giving its minimum size, it may include all the initially available acid monomers, i.e. 5 wt% of the particle content. Taking the same density and molar mass for MMA and MAA, this condition of maximum concentration of MAA in the core may be written as:

$$\frac{\frac{4}{3}\pi R_p^3 \rho}{M\ N_a} 0.05 < \frac{\frac{4}{3}\pi r_c^3 \rho}{M\ N_a}$$

with M the mean molar mass of a monomer, ρ the mean density and N_a the Avogadro number.

So, the lower limit of the particle core size is $(\frac{r_c}{R_p})^3 > 0.05$. The upper limit of r_c is given by the minimum size for the shell may be that of one layer of monomer that the size is around 10^{-9} m. Thus, the range of r_c allowed by these geometrical considerations is $0.999 > \frac{r_c}{R_p} > 0.37$. The use of these limits and equation 14 allow framing the concentration of acid in the shell c_L: $2\ 10^{-2}$ mol m^{-3} < c_L < 5 mol m^{-3} << c_H. This range is consistent with a low concentration of acid functions in the shell.

Estimation of D_{RCOONa}

The use of these limits and of the slopes from Figure 5 (Eq. 13), it can be deduced that:

$$D_{RCOONa} = \left(1 - \frac{r_c}{R_p}\right) \frac{\alpha'}{4\pi\ K\ R_p} \frac{R_p}{r_c}$$

R_p and α' are known.

c_H is approximatively equal to the number of acid groups divided by the volume of a particle. The number of acid groups $n_{tot} \times 5.8\%$ was already calculated, and then in the particle: $c_H \approx 1000$ mol m^{-3}. In the experiments carried out, $c_0 \leq 607$ mol m^{-3} thus $c_H > c_0$. Moreover, carboxylic

acids being relatively strong acids, it can be considered that almost no HO^- is present in the particle core. Then the constant K would be close to 1.
Putting all these results together it gives:
$7\ 10^{-25}\ \mathrm{m^2\ s^{-1}} < D_{RCOONa} < 8\ 10^{-22}\ \mathrm{m^2\ s^{-1}}$

These values are consistent with the diffusion coefficient of a polymer in its bulk below its glass transition temperature (36,37). The picture that emerges from modeling the kinetics of charge appearance is that the particle surface is made of a shell devoid of MAA, and that the kinetics of charge appearance in basic medium is set by the slowest migration phenomenon, namely the diffusion of charged polymeric species from the core to the surface.

4. Conclusion

The investigation into the mechanism of charges appearance at the surface of a-PMMA particles disclosed two simultaneous phenomena: the hydrolysis of ester functions and the deprotonation of acid groups.

The hydrolysis phenomenon studied on PMMA particles behave as a pseudo first-order reaction as long as the pH can be considered as constant.

The appearance of the surface charge coming from the neutralization of acid groups by NaOH was not instantaneous, suggesting that this acid-base reaction did not occur at the surface of the particles because the ionizable carboxylic acid groups were buried in the core of the particles. A model based on core-shell structure of the particles was proposed to explain the time dependence of charge appearance. The mechanism that led to charging the particles was mainly due to the neutralization and diffusion of acid functions buried into the particle rather than hydrolysis.

Anionic particles with controlled surface charge can be obtained by tempering the particles in alkaline conditions for a while and bringing them back to the desired lower pH. The tempering operating conditions in terms of pH and duration have been determined so as to keep a negligible hydrolysis of the ester functions at the particle surface. It is possible to expand the present method to obtain particles with a desired charge (positive or negative) with other sizes and other polymeric compositions. Cationic PMMA particles using another comonomer and an acid tempering were successfully prepared in the same way.

Conflict of interest

No conflict of interest has to be declared.

References

1. Honary S., Zahir F. (2013). Effect of zeta potential on the properties of nano-drug delivery systems - A review (Part 1). *Tropical J Pharm Res*, *12*(2), 255–264. https://doi.org/10.4314/tjpr.v12i2.19
2. Cai C., Bakowsky U., Rytting E., Schaper A.K., Kissel T. (2008). Charged nanoparticles as protein delivery systems: A feasibility study using lysozyme as model protein. *Eur J Pharm Biopharm*, *69*(1), 31–42. https://doi.org/10.1016/j.ejpb.2007.10.005
3. Song J., Kong H., Jang J. (2009). Enhanced antibacterial performance of cationic polymer modified silica nanoparticles. *Chem Commun*, 36, 5418–5420. https://doi.org/10.1039/b908060k
4. Croll T.I., O'Connor A.J., Stevens G.W., Cooper-White J.J. (2004). Controllable surface modification of poly(lactic-*co*-glycolic acid) (PLGA) by hydrolysis or aminolysis. I: Physical, chemical, and theoretical aspects. *Biomacromolecules*, *5*(2), 463–473. https://doi.org/10.1021/bm0343040
5. Tham C., Hamid Z.A.A., Ahmad Z., Ismail H. (2013). Surface engineered poly(lactic acid) (PLA) microspheres by chemical treatment for drug delivery system. *Key Eng Mater*, *594-595*, 214–218. https://doi.org/10.4028/www.scientific.net/KEM.594-595.214
6. Ladavière C., Averlant-Petit M.-C., Fabre O., Durand A., Dellacherie E., Marie E. (2007). Preparation of polysaccharide-coated nanoparticles by emulsion polymerization of styrene. *Colloid Polym Sci*, *285*(6), 621–630. https://doi.org/10.1007/s00396-006-1579-3
7. Lecomte F., Siepmann J., Walther M., MacRae R.J., Bodmeier R. (2004). Polymer blends used for the coating of multiparticulates: comparison of aqueous and organic coating techniques. *Pharm Research*, *21*(5), 882–890. https://doi.org/10.1023/b:pham.0000026443.71935.cb
8. Oukacine F., Morel A., Cottet H. (2011). Characterization of carboxylated nanolatexes by capillary electrophoresis. *Langmuir*, *27*(7), 4040–4047. https://doi.org/10.1021/la1048562
9. Vasiliu M.P., Sachelarie L., Romila L.E., Folescu E., Atanase L., Zaharia A. (2016). Surface state studies and biocompatibility of PMMA. *J Biomimetics Biomater Biomed Eng*, *28*, 57–65. https://doi.org/10.4028/www.scientific.net/JBBBE.28.57
10. Fleischmann S., Percec V. (2010). Copolymerization of methacrylic acid with methyl methacrylate by SET-LRP. *J Polym Sci Part A: Polym Chem*, *48*(21), 4884-4888. https://doi.org/10.1002/pola.2428
11. Rufino E. & Monteiro E. (2003). Infrared study on methyl methacrylate–methacrylic acid copolymers and their sodium salts. *Polymer*, *44*(23), 7189–7198. https://doi.org/10.1016/j.polymer.2003.08.041
12. Lee C.F., Hsu M.L., Chu C.H., Wu T.Y. (2014). Synthesis and characteristics of poly(methyl methacrylate-*co*-methacrylic acid)/poly(methacrylic acid-*co*-*N*-isopropylacrylamide) thermosensitive semi-hollow latex particles and their application to drug carriers. *J Polym Sci Part A: Polym Chem*, *52*(23), 3441–3451. https://doi.org/10.1002/pola.27411
13. Vargün E., Sankir M., Aran B., Sankir N.D., Usanmaz A. (2010). Synthesis and characterization of 2-hydroxyethyl methacrylate (HEMA) and methyl methacrylate (MMA) copolymer used as biomaterial. *J Macromol Sci, Part A*, *47*(3), 235–240. https://doi.org/10.1080/10601320903526998
14. Kang K., Kan C., Du Y., Liu D. (2005). Synthesis and properties of soap-free poly(methyl methacrylate-ethyl acrylate-methacrylic acid) latex particles prepared by seeded emulsion polymerization. *Eur Polym J*, *41*(3), 439–445. https://doi.org/10.1016/j.eurpolymj.2004.10.032
15. Daoust H., Rinfret M. (1952). Solubility of polymethyl methacrylate and polyvinyl acetate. *J Colloid Sci*, *7*(1), 11–19. https://doi.org/10.1016/0095-8522(52)90016-0
16. Lavielle L., Schultz J. (1985). Surface properties of graft polyethylene in contact with water. *J Colloid Interface Sci*, *106*(2), 438–445. https://doi.org/10.1016/s0021-9797(85)80017-5

17. Ohshima H., Healy T.W., White L.R. (1982). Accurate analytic expressions for the surface charge density/surface potential relationship and double-layer potential distribution for a spherical colloidal particle. *J Colloid Interface Sci*, *90*(1), 17–26. https://doi.org/10.1016/0021-9797(82)90393-9
18. Ibrahim A., Ohshima H., Allison S.A., Cottet H. (2012). Determination of effective charge of small ions, polyelectrolytes and nanoparticles by capillary electrophoresis. *J Chromatogr A*, *1247*, 154–164. https://doi.org/10.1016/j.chroma.2012.05.010
19. Ouadah N., Doussineau T., Hamada T., Dugourd P., Bordes C., Antoine R. (2013). Correlation between the charge of polymer particles in solution and in the gas phase investigated by zeta-potential measurements and electrospray ionization mass spectrometry. *Langmuir*, *29*(46), 14074–14081. https://doi.org/10.1021/la403516y
20. Jalil A.H., Pyell U. (2018). Quantification of zeta-potential and electrokinetic surface charge density for colloidal silica nanoparticles dependent on Type and concentration of the counterion: probing the outer Helmholtz plane. *J Phys Chem C*, *122*(8), 4437–4453. https://doi.org/10.1021/acs.jpcc.7b12525
21. Biroš J., Larina T., Trekoval J., Pouchlý J. (1982). Dependence of the glass transition temperature of poly (methyl methacrylates) on their tacticity. *Colloid Polym Sci*, *260*(1), 27–30. https://doi.org/10.1007/bf01447672
22. Grohens Y., Brogly M., Labbe C., David M.O., Schultz J. (1998). Glass transition of stereoregular poly(methyl methacrylate) at interfaces. *Langmuir*, *14*(11), 2929–2932. https://doi.org/10.1021/la971397w
23. Smitz L., Schmitz V. (1988). The effect of water on the glass transition temperature of poly(methyl methacrylate). *Polymer*, *29*(10), 1871–1878. https://doi.org/10.1016/0032-3861(88)90405-3
24. Brandrup J., Immergut E.H., Grulke E.A. (1999). *Polymer Handbook*. Wiley. p 203.
25. Ma H., Luo M., Dai L.L. (2008). Influences of surfactant and nanoparticle assembly on effective interfacial tensions. *Phys Chem Chem Phys*, *10*(16), 2207–2213. https://doi.org/10.1039/b718427c
26. Kirby B.J., Hasselbrink E.F. (2004). Zeta potential of microfluidic substrates: 2. Data for polymers. *Electrophoresis*, *25*(2), 203–213. https://doi.org/10.1002/elps.200305755
27. Glass R.L. (1971). Alcoholysis, saponification and the preparation of fatty acid methyl esters. *Lipids*, *6*(12), 919–925. https://doi.org/10.1007/bf02531175
28. Kurenkov V.F., Hartan H.G., Lobanov F.I. (2001). Alkaline hydrolysis of polyacrylamide. *Russ J Appl Chem*, *74*(4), 543–554 https://doi.org/10.1023/a:1012786826774
29. Ivanova T., Panaiotov I., Boury F., Proust J., Benoit J., Verger R. (1997). Hydrolysis kinetics of poly(d,l-lactide) monolayers spread on basic or acidic aqueous subphases. *Colloids Surfaces B: Biointerfaces*, *8*(4-5), 217–225. https://doi.org/10.1016/s0927-7765(96)01331-8
30. Casalini T., Rossi F., Lazzari S., Perale G., Masi M. (2014). Mathematical modeling of PLGA microparticles: from polymer degradation to drug release. *Mol Pharm*, *11*(11), 4036–4048. https://doi.org/10.1021/mp500078u
31. Siepmann J., Elkharraz K., Siepmann F., Klose D. (2005). How autocatalysis accelerates drug release from PLGA-based microparticles: a quantitative treatment. *Biomacromolecules*, *6*(4), 2312–2319. https://doi.org/10.1021/bm050228k
32. Atkin R., Davies P., Hardy J., Vincent B. (2004). Preparation of aqueous core/polymer shell microcapsules by internal phase separation. *Macromolecules*, *37*(21), 7979–7985. https://doi.org/10.1021/ma048902y

33. Yasuda H., Lamaze C.E., Ikenberry L.D. (1968). Permeability of solutes through hydrated polymer membranes. *Makromol Chem*, *118*(1), 19–35. https://doi.org/10.1002/macp.1968.021180102
34. Unemori M. (2003). Water absorption of poly(methyl methacrylate) containing 4-methacryloxyethyl trimellitic anhydride. *Biomaterials*, *24*(8), 1381–1387. https://doi.org/10.1016/s0142-9612(02)00521-5
35. Zhang H., Lamnawar K., Maazouz A. (2012). Rheological modeling of the diffusion process and the interphase of symmetrical bilayers based on PVDF and PMMA with varying molecular weights. *Rheol Acta*, *51*(8), 691–711. https://doi.org/10.1007/s00397-012-0629-7
36. Ehlich D., Sillescu H. (1990). Tracer diffusion at the glass transition. *Macromolecules*, *23*(6), 1600–1610. https://doi.org/10.1021/ma00208a008
37. Boiko Y.M. (2014). On the continuity of the diffusion behaviour at amorphous polymer–polymer interfaces on both sides of the bulk glass transition temperature. *Colloid Polym Sci*, *292*(7), 1719–1723. https://doi.org/10.1007/s00396-014-3238-4

Supplementary information

Supplementary Information 1: NMR results

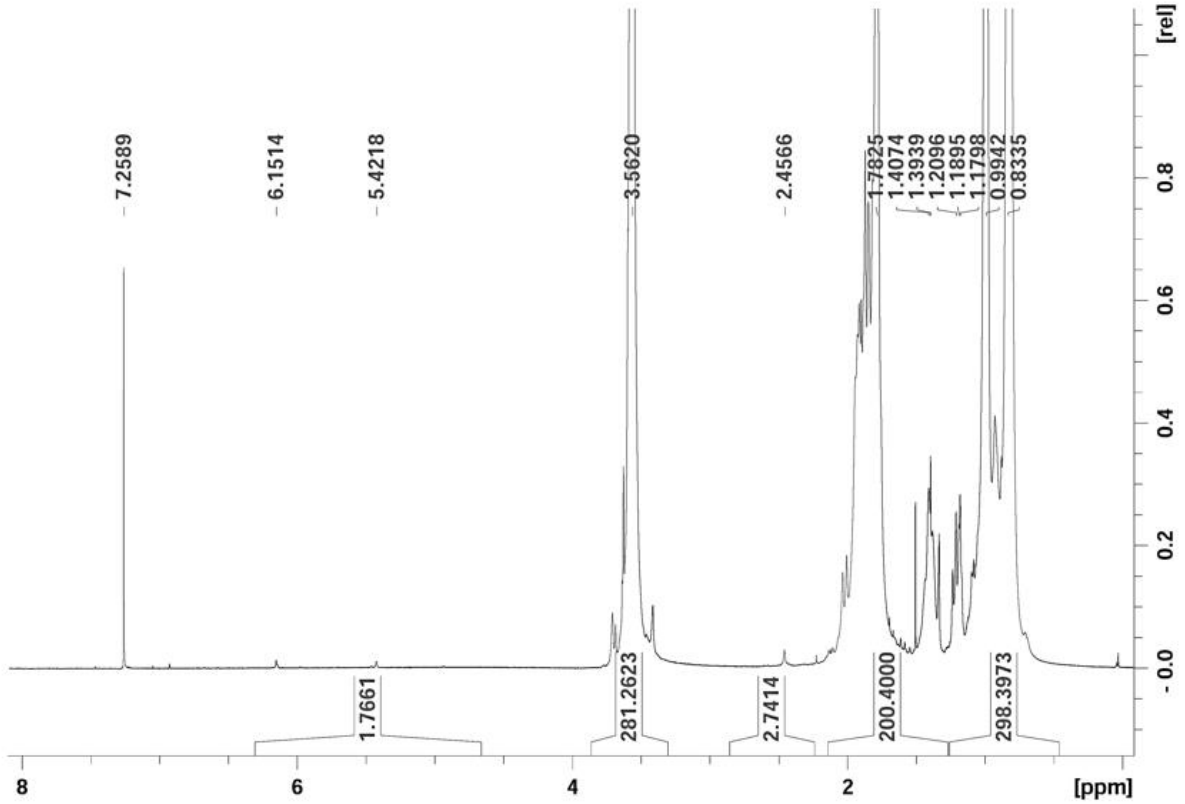

Figure S1. ^{1}H NMR spectrum of the PMMA-*co*-MAA polymer (at 60 °C).

The two peaks that characterize the C=C chemical bond in the monomers is supposed to appear around 5.6 and 6.2 ppm. When a good polymerization occurs, these peaks disappear. In this case, the polymerization has occurred as expected and almost no residue was detected.

Supplementary Information 2*: DSC results*

Pure PMMA polymer

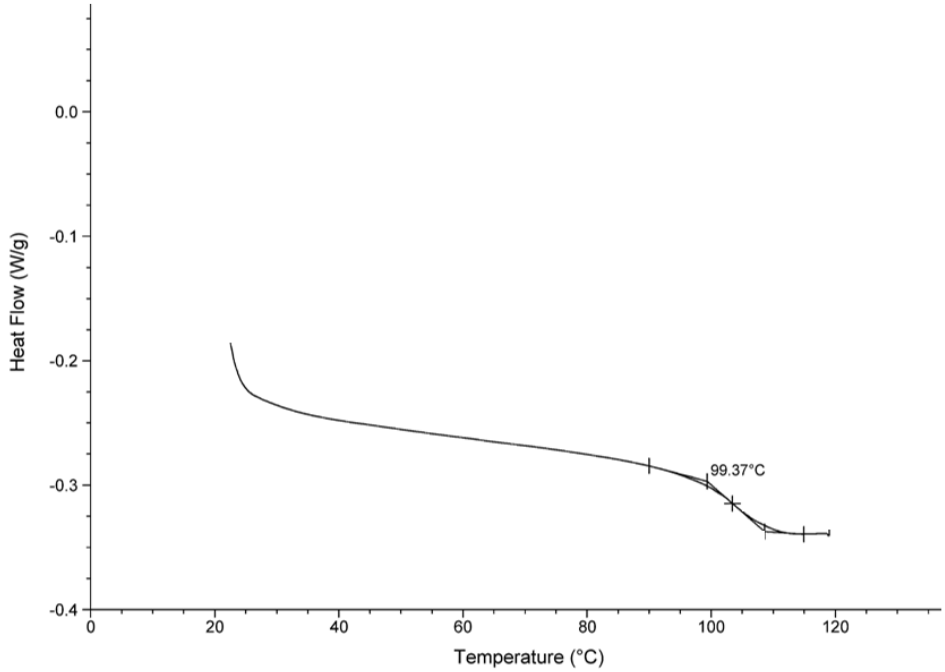

$PMMA_{95\%}$-co-$MAA_{5\%}$ polymer

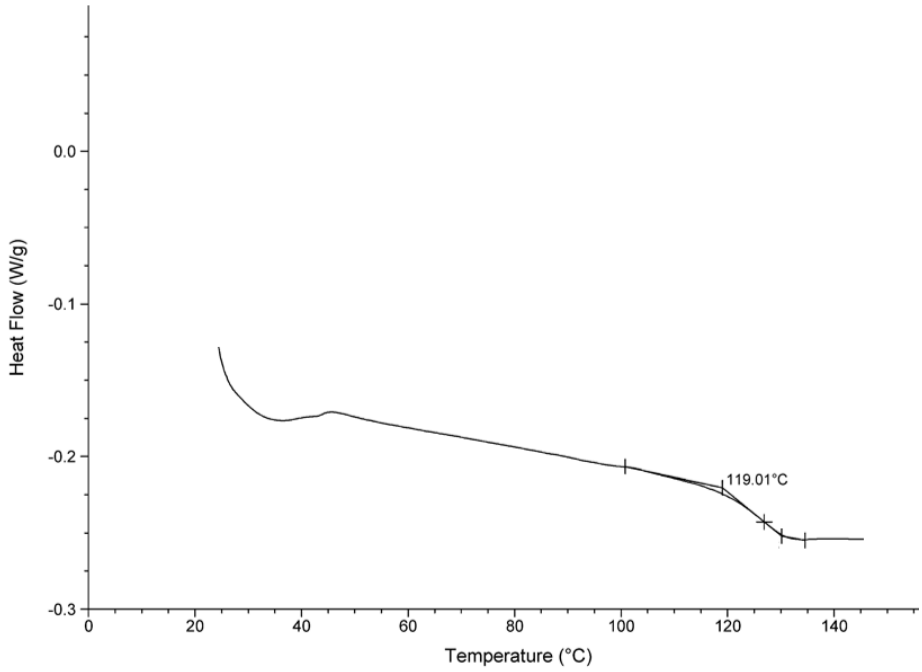

Figure S2. DSC measurements for both polymers.

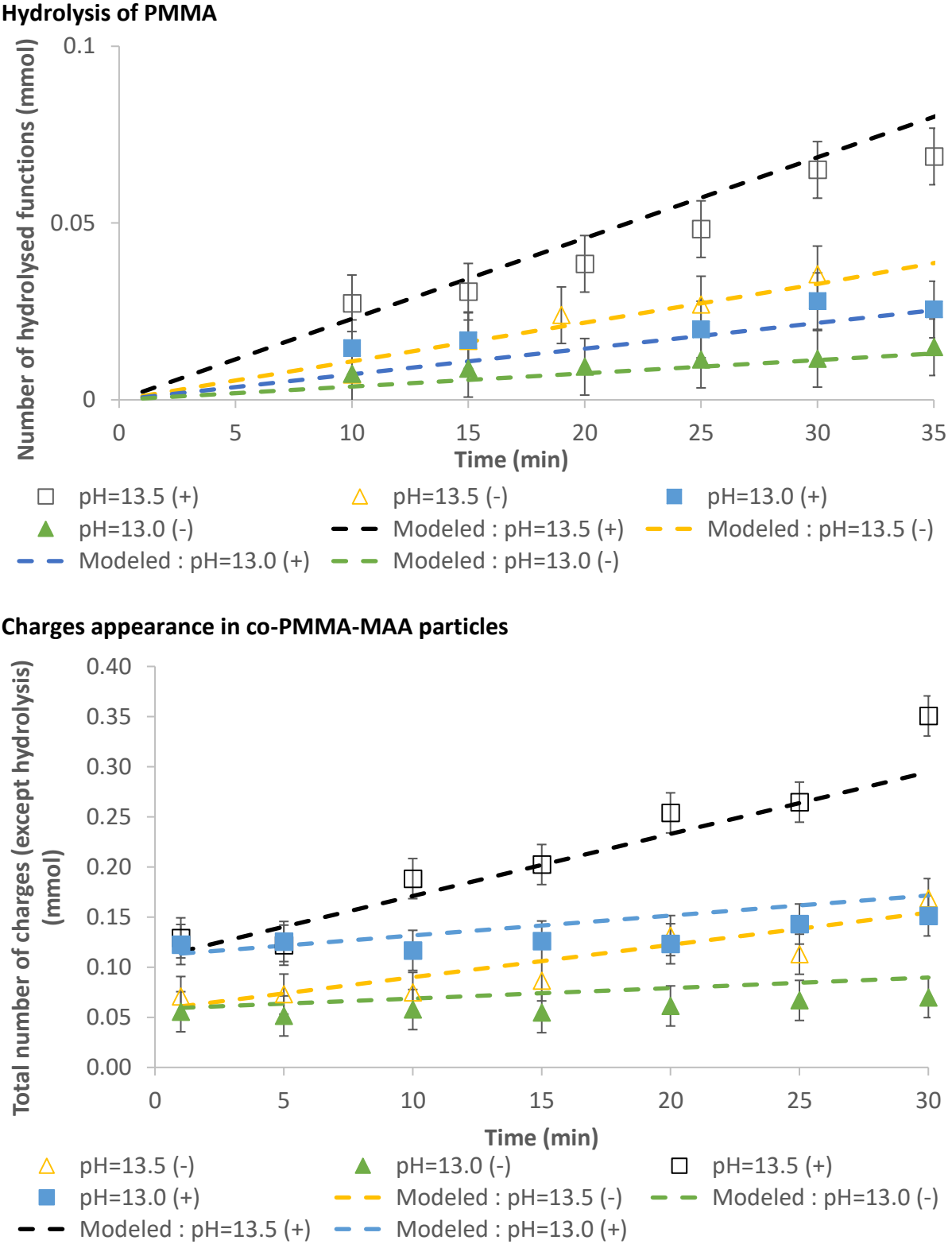

Figure S3. Hydrolysis measurements comparison with the models predictions.

Supplementary Information 4: Example of ANCOVA test for 2 linear regressions (testes made on the total number of charge appearance)

An Analysis of Covariance (ANCOVA) test was performed to compare the *y*-intercepts and the slopes of the linear regression models used for the fitting of the kinetics of the surface charge appearance. In an ANCOVA, the first step is to test the null hypothesis that the slopes of the regression lines are equal. If the slopes are not significantly different, the second null hypothesis that the *y*-intercepts of the regression lines are the same has to be tested. We used here the data that have been determined at pH 13.5 (-) and pH 13 (-) to illustrate the ANCOVA (cf Figure 5).

pH	Time (min)	Number of charge
13.5 (-)	1	8.12 E+02
13.5 (-)	5	8.40 E+02
13.5 (-)	10	8.59 E+02
13.5 (-)	15	9.92 E+02
13.5 (-)	20	1.51 E+03
13.5 (-)	25	1.30 E+03
13.5 (-)	30	1.93 E+03
13 (-)	1	6.30 E+02
13 (-)	5	5.83 E+02
13 (-)	10	6.55 E+02
13 (-)	15	6.20 E+02
13 (-)	20	6.96 E+02
13 (-)	25	7.59 E+02
13 (-)	30	7.91 E+02

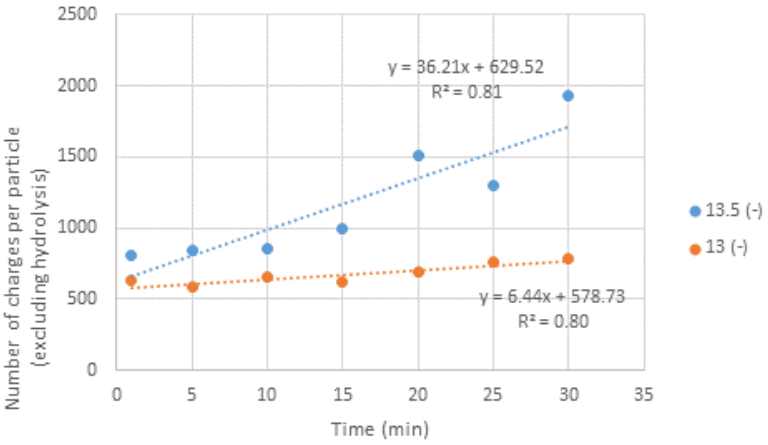

From these data, two linear regression lines were fitted (k = 2, slope$_1$ = 36.21 and slope$_2$ = 6.44) and the residual sum of squares (SS_R) was determined for each model as:

$$SS_R = \sum_{i=1}^{N} (y_i - \hat{y}_i)^2$$

with N the number of experiments (N = 7), y_i and $\hat{y}_i$ respectively the experimental and the predicted numbers of charge for experiment i.

The variation which was not explained by the two regression lines is $SS_{RT} = SS_{R1} + SS_{R2}$ = 208159.

Considering two parallel regression lines characterized by a slope equal to the average of slope$_1$ and slope$_2$ (slope$_{ave}$ = 21.33), we obtained a residual sum of squares $SS_{RT,ave.s} = SSR_{1ave.s} + SSR_{2ave.s}$ = 2070600.

The residual error due to the variation of the slopes is $SS_{Rv.s} = SS_{RT,ave.s} - SS_{RT}$- = 1862439.

To test the null hypothesis that the slopes of the regression lines are equal, we compared the residual variances obtained from $SS_{Rv.s}$ and SS_{RT} using a *F*-test:

$F = \frac{SS_{Rv.s}/(k-1)}{SS_{RT}/(N-2k)}$ = 89 that corresponds to a *p*-value of 3.10^{-6}.

The *p*-value being below the risk (5%), the null hypothesis is rejected indicating that the slopes are statistically different.

In the case of similar slopes, we tested the second null hypothesis that the y-intercepts of the regression lines are the same. A unique regression line has to be determined and allows the determination of the residual sum of squares $SS_{R,ave.int}$.

The residual error due to the difference between the *y*-intercepts was determined $SS_{Rv.int} = SS_{R,ave.int} - SS_{RT,ave.s}$. The corresponding variance is finally compared to the one obtained from $SS_{RT,ave.s}$ using a *F*-test.